Composites Science and Technology 71 (2011) 1898–1907. doi: 10.1016/j.compscitech.2011.09.004

A cohesive zone model for predicting delamination suppression in z-pinned laminates

Francesco Bianchi, Xiang Zhang*

Aerospace Engineering Dept, School of Engineering, Cranfield University, MK43 0AL, UK

Abstract

This paper presents a cohesive zone model based finite element analysis of delamination resistance of z-pin reinforced double cantilever beam (DCB). The main difference between this and existing cohesive zone models is that each z-pin bridging force is governed by a traction-separation law derived from a meso-mechanical model of the pin pullout process, which is independent of the fracture toughness of unreinforced laminate. Therefore, two different traction-separation laws are used: one representing the toughness of unreinforced laminate and the other the enhanced delamination toughness owing to the pin bridging action. This approach can account for the large scale bridging effect and avoid using concentrated pin forces, thus removing the mesh dependency and permitting more accurate analysis solution. Computations were performed using a simplified unit strip model. Predicted delamination growth and load vs. displacement relation are in excellent agreement with the prediction by a complete model, and both models are in good agreement with test measured load vs. displacement relation. For a pinned DCB specimen, the unit strip model can reduce the computing time by 85%.

Keywords: z-fibre pinning, delamination, large scale bridging, traction separation law.

1. Introduction

To improve the delamination resistance in carbon fibre reinforced composites, several through-thickness reinforcement techniques have been developed, e.g. stitching [1], z-fibre pinning (or z-pinning) [2-5], and tufting [3, 6]. Stitching and tufting are effective toughening methods, but can only be applied to composites made from resin infused fabric preforms. Z-pinning has attracted larger interest in its application in the aircraft structures, because it is the only through-thickness toughening technique that can be readily applied to composite joints made of prepreg materials. When a delamination crack propagates, z-pins provide traction forces that restrict the crack opening displacement and increase the fracture toughness [7, 8].

A number of models have been developed for predicting delamination suppression in z-pinned laminates. These models are either analytical [9-13] or numerical using the finite element method [7, 14-16]. Z-pin bridging effect is modelled by averaging the bridging forces over the entire reinforced area [9-12,14-16], or by the classic beam theory [11-13], or nonlinear springs exerting concentrated traction force at the pin location [7, 13-14, 17]. A review of these approaches is given in Section 2.2. However, using average surface traction forces is more appropriate for tufted or stitched laminates due to the smaller diameter and

* Corresponding author

Email addresses: xiang.zhang@cranfield.ac.uk (X. Zhang); f.bianchi@cranfield.ac.uk (F. Bianchi)

closer distance of these reinforcement threads. Since the space between adjacent z-pins is usually much larger causing the characteristic slip-stick behaviour, enhanced fracture toughness is not best represented by the average fracture toughness. On the other hand, using concentrated pin forces in models can cause stress singularity problem and consequently the computational solution can be mesh dependent. To overcome these difficulties, cohesive zone models (CZM) have been used recently for modelling adhesive failure or delamination in unpinned laminates with encouraging results [17-22]. Compared with alternative analysis techniques such as the virtual crack closure technique (VCCT) [23, 24], CZM has the capability to model both crack initiation and crack propagation.

This paper presents a cohesive zone finite element model for predicting progressive delamination in z-pinned laminate. It is different from the current methods in the open literature that use either average value of enhanced fracture toughness or CZM for unpinned area only. Rather, two separate cohesive laws are employed to represent the delamination toughness of the unpinned and pinned areas, respectively. The local forces exerted by pins can better represent the large scale bridging effect without introducing stress singularities.

2. Background

2.1. Energy balance during crack bridging

For crack extension *da*, the strain energy release rate *G* can be expressed as:

$$G = -\frac{d\Pi}{da} = \frac{1}{B}\left(\frac{dW}{da} - \frac{dU}{da}\right) \tag{1}$$

where $d\Pi$, dW and dU are respectively the increase of the potential energy, work done by external force and elastic strain energy of the system, and B the width of test specimen.

The critical strain energy release rate $\left(G_C^{total}\right)$ required for unit crack extension in pinned laminates can be regarded as the sum of two contributions: the material intrinsic fracture toughness needed for creating new crack surface $\left(G_C\right)$ and the increased energy dissipation rate due to z-pin bridging effect $\left(G_C^{pin}\right)$, eq. (2):

$$G_C^{total} = G_C + G_C^{pin} \tag{2}$$

According to the Griffith theory [25], fracture occurs when:

$$G \geq G_C + G_C^{pin} \tag{3}$$

Fracture toughness of unpinned laminate G_C is a material property, but the energy dissipation rate due to the pins G_C^{pin} is a material-structure attribute that depends also on the pin geometry

and insertion density, as well as the crack opening displacement. G_C^{pin} is mostly due to the energy absorption during the pin's frictional pullout process and can be calculated by:

$$G_C^{pin} = \frac{1}{B}\frac{d\left(\sum_i \int P_i(u_i)du_i\right)}{da} \tag{4}$$

where P_i is the bridge force exerted by an active z-pin in the crack wake and u_i the crack opening displacement at the respective pin location.

For a fracture process such as in-plane fibre bridging characterised by having a crack wake bridging area that is smaller than any other specimen dimension, the delamination suppression mechanism is called small scale bridging (SSB). For stitched, tufted and z-pinned laminates, due to the pin frictional pullout process, the bridging length is usually of the same order of the laminate thickness resulting in the so-called large scale bridging (LSB) mechanism. Some researchers consider the bridging effect provided by the through-thickness reinforcements to have a constant bridging length and therefore, G_C^{total} can be calculated by averaging the energy dissipation rates over the reinforced area [10, 17]. However, this assumption seems more appropriate for SSB than LSB; in the latter case the pin bridging force varies during the fracture process and thus, G_C^{total} is not a constant value. Therefore, enhanced fracture toughness should be evaluated by accounting for the two energy contributions separately [7].

2.2. *Existing z-pin models*

Experimental and theoretical analyses have been performed on z-pinned laminates under the mode-I, mode-II and mixed mode load conditions [4, 5, 8]. Models have been developed to predict the enhanced fracture toughness and suppressed delamination crack growth rate under the mode-I load condition. Two main approaches are: (1) z-pin forces are averaged over the bridging area and their contribution is counted as traction force, which is function of the local delamination displacement [9, 10, 12]; (2) each pin traction is treated as a concentrated force acting at the pin location and governed by a non-linear force-displacement relation [7, 11, 17, 26]. When the first approach is employed, the bridging relation is defined as either a stress-displacement relation [9, 10] or the stiffness of an elastic foundation [12].

The use of CZM to model delamination and adhesive failure has yielded encouraging results. Owing to the mixed strength/energy based failure criterion, initial crack is not needed in the model. The CZM approach is different from the classic fracture mechanics, postulating that crack initiation and growth is no longer a sudden or abrupt event, but a gradual degradation process of the material ahead of the crack tip until complete failure. CZM can be readily

implemented into a FEM code. The zone ahead of the crack tip is called the process zone. The traction between the two crack surfaces is described as a function of the crack opening displacement and the relation is usually referred as the traction-separation law (TSL). CZM has been used for modelling delamination of unpinned laminates under the mode-I, mode-II and mixed mode I/II loading conditions with encouraging results [18, 20, 21]. Recently, attempts have been made to use CZM to model through-thickness reinforcement in mode-I condition. Sun and Jin developed a FE model using a cohesive-bridging law to account for the energy contribution due to in-plane fibre bridging [19]. A similar approach was adopted by Dantuluri et al. to simulate delamination in z-pinned double cantilever beam (DCB) [17]. However, the TSL used in both works was based on the average value of strain energy dissipation rate due to the pins over the whole fracture surface. This kind of approach is more suitable to the SSB where the energy contribution due to bridging can be considered as an improved material property.

Ratcliffe and O'Brien developed an analytical model of z-pinned DCB using discrete springs with a bilinear damage model, similar to the CZM approach, to model the pin progressive pullout from a laminate [13].

2.3. *Z-pin failure process*

In some models, traction force exerted by z-pin is treated as a function of the displacement between the two surfaces of delamination crack whether or not the force is averaged over the bridging length. This bridging-law can be obtained from a single-pin pullout specimen by either experimental testing [4] or numerical modelling [27]. Models have been developed for the mode I, mode II, and mixed mode load conditions [10, 28-31].

There are three phases in z-pin bridging process: (1) pin is initially stretched under the applied load, (2) pin then debonds from the surrounding laminate, and (3) pin is progressively pulled out due to increasing delamination displacement. The shear stress at the pin/laminate interface is the main mechanism putting the pin under axial stress. The cohesion is initially due to the chemical bond and then the friction resistance caused by the contact stresses (thermal residual stresses) at the pin/laminate interface induced by the curing process at elevated temperature. Experimental tests have shown that only one side of the pin slides out while the other side remains anchored to the laminate. Usually the side with the chamfer head (used to facilitate pin insertion) is more likely to debond and then be pulled out [4].

The debonding phase starts as soon as the maximum shear stress reaches the shear strength of the bond interface. The average shear stress τ_a at the disbond onset and the corresponding maximum pullout force are, respectively:

$$\tau_a = \frac{1}{h^*}\int_0^{h^*} \tau(z)dz, \quad P_{\max} = \pi d h^* \tau_a \tag{5}$$

where $\tau(z)$ is the shear stress variation along the pin surface, d is the pin diameter, h^* is the embedded pin length between the laminate delamination plane and the pin chamfer end.

The pin pullout phase takes place immediately after the disbond onset. The average friction stress τ_f and the maximum pullout force $P_{\max,f}$ at the beginning of the pullout are respectively:

$$\tau_f = \frac{1}{h^*}\int_0^{h^*} \tau(z)dz, \quad P_{\max,f} = \pi d h^* \cdot \tau_f \tag{6}$$

Fig. 1 shows two typical pin pullout behaviours observed from experiments [4, 32]. First, the pullout force will reach its maximum, at which point disbond occurs at the pin/laminate interface. After this point there could be a sudden load drop before the frictional pullout phase (Fig. 1a) depending on the friction resistance that can be represented by the ratio of τ_a/τ_f. Force drop occurs if the ratio is great than one; and the higher the ratio, the larger the drop. If $\tau_a/\tau_f \leq 1$, then there is no sudden force drop and the force vs. displacement curve has a characteristic bilinear shape (Fig. 1b).

3. Modelling strategy

The objective of this research is to develop a FEA tool using the cohesive zone model (CZM) for predicting progressive delamination growth under the z-pin bridging effect. The modelling strategy is presented in Fig. 2. The idea is to use a respective CZM law for the unpinned area and pinned locations. The unpinned CZM is governed by the laminate intrinsic toughness, whereas enhanced delamination toughness due to the pin bridging is used in the pin locations.

To realise this goal, multi-scale models have been developed. Firstly, the pin bridging force is evaluated by a meso-mechanical model of single-pin pullout process. The resultant bridging law is then implemented into a macro-scale structural model at each pin location.

This approach can account for the local effect caused by z-pins, avoiding either averaging the pin forces over the whole reinforcement area or using concentrated traction forces. The large scale bridging effect of pins is therefore better represented, especially for lower pin densities, permitting more accurate analysis. This work is aimed at the mode I load condition, but it

should be possible for the model to be further developed to the mode II and mixed mode conditions by using corresponding pin bridging laws.

4. Single-pin pullout model (meso-scale)

4.1. *Model assumption*

Numerical model presented here is taken from the experimental test published in [4]. Test specimen was made of 32 unidirectional plies of IMS/924 prepreg resulting in 4 mm nominal thickness. A thin film was inserted in the mid plane to separate the laminate into two halves to avoid any interaction between the two parts. A z-pin of 0.51 mm diameter was inserted by an ultrasonic hammer. A 10 x 10 mm test piece was then cut off with the z-pin positioned in the middle as shown in Fig. 3a. Two end-tabs were bonded to the laminate free surfaces to facilitate load application in the test machine. The test was performed under displacement-controlled loading condition and the resultant force was recorded.

Only the part of the specimen in the half containing the pin chamfer tip was modelled as indicated in Fig. 3b. The chamfer is not considered to influence the pin pullout resistance; hence the model thickness (h^*) is reduced by the height of the chamfer (d). The rest part of the specimen beyond the model domain is assumed to have linear elastic behaviour that was modelled by an elastic spring with stiffness k. Fig. 4a shows half of the model domain due to symmetric geometry.

An axi-symmetric FE model was used as shown in Fig. 4. It is based on the observation of a resin-rich pocket around the pin, of about 5-6 pin diameters, caused by the pin insertion. Considering that laminate properties in the cross fibre direction are dominated by the resin matrix, material surrounding the pin is assumed as homogeneous and isotropic.

Experimental observation has pointed out that the initial debonding phase gives a negligible contribution to the energy absorption, therefore the pullout resistance is considered being caused by the friction force only [9, 27]. This friction resistance results from the compressive residual stresses around the pin due to the curing process. Since the coefficient of thermal expansion of the carbon-fibre pin is a magnitude smaller than that of the surrounding resin dominated material, the resin matrix shrinks more than the pin after cooling down from the elevated cure temperature to room temperature, resulting in compressive residual stress acting along the pin in the radial direction.

The model uses a surface to surface algorithm to calculate the normal contact stress and the coulomb friction. The curing process is modelled by applying a temperature change from 180°C to 25°C. Thermal residual stresses are calculated and saved in the model as the initial

condition in order to maintain displacement compatibility. A pullout force is then applied at the pin top surface under the displacement controlled loading condition. Numerical simulation runs until the pin is completely pulled out.

It should be noted that the main energy dissipation mechanism accounted by this model is the friction resistance during the z-pin pullout process. However, when pins are inserted into a thicker laminate (e.g. > 8-10 mm), pin's failure mode may switch from pullout to pin rupture. The latter failure mode is not accounted for by the present model, which limits the model's application to only the thinner laminates. However, energy dissipation in the pin final rupture failure is much smaller than that in the pin pullout process.

4.2. *Numerical results*

Commercial FE software package ABAQUS v6.9 was used for the analysis. Axi-symmetric quadrilateral quadratic elements (CAX8) are used in the model. Converged numerical results were achieved uisng the mesh shown in Fig. 4b; a refined mesh at pin-laminate interface, where the stresses are higher, and a relatively coarse mesh away from it. Material properties used in the analysis are given in Table 1 (z-pin) and Table 2 (laminate). Mechanical properties of the pin's surrounding laminate material used in the single-pin model are: E = 11 GPa, ν = 0.4 and coefficient of thermal expansion $\alpha = 2.4 \times 10^{-5}$ K^{-1}. Although pin's surrounding material is mainly the resin matrix, the mechanical property is not the same as the pure resin due to the existence of fibres. Therefore, laminate transverse properties were used for the material close to the pin. The temperature difference applied to simulate the curing process is -155°C. Residual stress field is a function of the temperature change, model dimension, coefficients of thermal expansion and Young's modulus of the pin and surrounding material in the radial direction.

The normal and shear stresses along the pin/laminate interface are presented in Fig. 5. Following observations can be made. First, curing process induced thermal residual stress in the pin's lateral direction (σ_r) is negative, about 30 MPa, indicating that the pin is under compression by surrounding materials. This initial contact stress causes friction resistance when a pullout load is applied. The residual shear stress (τ_{zr}) is a balanced distribution of 15 MPa. Second, at the maximum applied load, the surrounding laminate is subjected to shear deformation resulting in the pin under high shear stress at the pin end (Fig. 5b), which in turn increases the contact pressure at the lower part of the pin (Fig. 5a). This increased contact pressure adds extra resistance to the pin pullout. The level of this contact stress is related to the laminate shear deformation, which depends on the aspect ratio of embedded pin length to

pin diameter, h^*/d (Fig. 3b). Therefore, the average friction resistance cannot be regarded as a constant for different geometries. Fig. 6 shows the dependency of average shear stress on the ratio h^*/d. The larger the ratio, the lower the average shear stress will be.

Calculated pin pullout force vs. displacement relation under displacement controlled loading condition was correlated with the test measurement in [4] in order to calibrate two constants used in the numerical model: the stiffness of the elastic spring (k), see Fig. 4(a), and the friction coefficient (μ). Parameter k influences mainly the initial slope, whereas μ affects the slope of the second part of the curve. With k = 200 kN/m and μ = 0.75, the model agrees with the test result very well as shown in Fig. 7a. These two parameters were then kept constant to evaluate z-pin bridging forces of other geometries. The curve's second part where the pin is progressively pulled out of the laminate has a constant descending slope until the last point where the pullout force suddenly drops to zero. This is due to the much lower contact stresses close to the laminate free surface and the consequently much reduced friction resistance (Fig. 5a).

Fig. 7b is a schematic of the traction-separation law, i.e. cohesive zone model, describing the pin bridging effect. It is deduced from the pin pullout force vs. displacement relation in Fig. 7a. The law is defined by three parameters, i.e. the initial stiffness (K), the cohesive strength (T_0) and the fracture toughness (G_C^{pin}). This law can be implemented into a macro-scale structural model (DCB in this paper) for calculating delamination growth in pinned laminates.

5. DCB model (macro-scale)

5.1. Geometry and model description

Pinned and unpinned DCB test specimens taken from [5] were modelled. Geometry and dimension are shown in Fig. 8. Each specimen was made of 24 plies of unidirectional prepreg of IMS/924 resulting in 3 mm nominal thickness[†]. Mechanical properties of the laminate are summarised in Table 2. An initial crack of 50 mm length was made by inserting a thin polyamide film in the mid-plane of the specimen. Z-pins were made of pultruded T300/BMI. Pinned area starts 5 mm from the initial crack tip[‡] lasting 25 mm in length and covering the entire specimen width. Three pin configurations of variable pin diameter and pin areal density were modelled; these parameters are summarised in Fig. 8 insert.

Two different FE models have been developed: a complete model (referred as "whole" model in this paper) representing half of the specimen geometry (Fig. 9a), and a simplified "unit

[†] Measured laminate thickness is 3.2 mm for unpinned and 3.3 for pinned specimens.

[‡] The distance of reinforced area from initial crack tip is only 1 mm in the configuration 3 specimen (as labelled in Fig. 8).

strip" model (Fig. 9b) by exploiting the periodic pin arrangement. The unit strip represents one half of a pin row in the mid-width and the surrounding laminate of the dimension of a periodical repeating unit. The *y*-axis deformation is constrained; hence it neglects the free-edge effects. However, the much reduced model size allows significant saving in computational effort. In both models, 8-node linear continuum shell elements with reduced integration (designated as CS8R in ABAQUS) were used for the laminate beams and 8-node cohesive elements (COH8) for the bonding interface. Element size in cohesive zone is one fifth of the adjacent shell element (Fig. 9 insert), in order to achieve numerical stability. This is essentially a 2D shell element model using one layer shell elements for each DCB arm and cohesive elements for the interface. The 3D view shown in Fig. 9 is a feature of the ABAQUS "continuum shell" element that has independent displacement degree of freedom enabling calculation of the rotation variables from the difference in nodal displacement between the element top and bottom surfaces.

Cohesive elements at the interface are governed by two different traction-separation laws: one for the unpinned laminate toughness and the other for pin enhanced toughness. For the unpinned laminate, published test data of unreinforced DCB were used to correlate the cohesive model parameters. Parameters of the bridging cohesive law were calculated by dividing the pin pullout force by the pin cross section area.

$$T(u) = \frac{P(u)}{\pi d^2 / 4} \tag{7}$$

where u is the delamination opening displacement, $T(u)$ is the bridging stress in the cohesive law and $P(u)$ is the pullout force (derived from the meso-mechanical model). Fig. 7b shows a sketch of the traction-separation law indicating the physical meaning of the three parameters in a cohesive model. Values of these parameters used in the analyses are given in Table 3.

In the whole model a symmetric boundary condition is applied along the longitudinal plane. Boundary conditions of the unit strip model are set according to the pin periodic arrangement, i.e. the two longitudinal planes that delimit the unit strip are constrained in the *y*-axis direction. For both models load is applied by displacement controlled condition, i.e. a separation displacement δ is imposed at the delamination mouth.

5.2. *Numerical results*

Calculated force vs. displacement and crack extension vs. applied displacement for the three pin configurations and comparison with the test results in [5] are presented in Figs. 10 – 12. The first two cases (pin areal density A_p= 2% with pin diameter d = 0.51 mm, and A_p= 0.5% with d = 0.28 mm) were simulated by both the whole and unit strip models; the third case

(A_p= 2% with d = 0.28 mm) was modelled only by the unit strip model due to the excessive computational cost of the complete model.

All three cases show similar trends in the load-displacement curves that are also plotted together in Fig. 13. Following observations are made. First, an elastic response is observed at the beginning, and the initial delamination crack starts propagating at the same load level (about 41 N) for the pinned and unpinned specimens. This indicates that initial delamination growth before the crack tip entering the pinned region is controlled by the toughness of the plain resin regardless the specimen is pinned or not. Second, as soon the delamination crack starts growing the load has a small drop (at about 41 N). For the unpinned specimen the load decreases from here continuously and monotonically after the peak, whereas all pinned specimens can recover after the small load drop and pick up much more loads. Pin bridging effect starts as soon as the delamination crack passes the first pin row. Crack tip is shielded from the crack opening force when pins are bridging the crack wake; consequently crack growth slows down (Fig. 13b) and the load recovers from the small drop at the delamination onset and increases to a maximum. Third, the crack bridging length is a good indicator of the bridging effect. The parameter is defined as the length of the crack wake where the pins are still active, i.e. not yet being pullout completely. This information is presented in terms of the number of active pin rows indicated on the right-hand-side *y*-axis of Figs.10a−12a. It shows that the bridging length increases as the number of active pins rises. Active pin number reaches a saturate value at the maximum load; from this point onwards, whenever the delamination crack passes a new pin row, pins in the far end row of the bridging area will be pulled out, maintaining the “active” pin number almost constant. However, the bridging force of the active pins in the crack wake is not constant during delamination growth. This causes the characteristic “slip-stick” behaviour, which is demonstrated by the oscillating force curve after the peak force.

For the same specimens, crack extension length vs. applied displacement is plotted in Figs. 10b-12b and also in Fig. 13b. It should be pointed out that in the experiment crack lengths were measured by visual observation; therefore the comparison of this parameter may be more qualitative than quantitative. For all three cases delamination crack starts growing at the same applied displacement. After an initial fast growth, crack growth rate become much slower in the first stage when the number of “active” pin at the crack wake increases. After the peak force, crack growth rate increases again. Final unstable failure occurs when the crack tip passes the pin reinforced area and the number of active pins in the crack wake drops to zero.

In all three cases the model has slightly underestimated the load capability, i.e. the model is conservative, with an error range of 5-10% (Fig. 13a). For the crack extension prediction (Fig. 13b), discrepancy between the model and experiment is much larger especially at the early crack growth stage (Δa = 0-15 mm), after which the model and experimental results are in reasonably good agreement.

Fig. 14 shows the values of interlaminar peel stresses at the delamination plane during the steady crack growth stage at applied displacement δ = 25 mm (for z-pin parameter A_p=2%; d=0.51 mm). It demonstrates that active pins in the crack wake shield the crack from suffering the full crack opening displacement. Consequently the pins are subject to high peel stresses. The whole model predicts faster crack growth at the specimen centre (on the longitudinal symmetry plane) as depicted crack front profiles in Fig. 14a. Since the unit strip model represents a centre strip of the specimen containing the mid-row pins and neglects the free edge effect, the modelled crack front is just the crack tip position. Both models predict a bridging length equal to four pin pitch size (as indicated by the four active pins subjected to tensile stress), demonstrating therefore the large-scale bridging scenario.

Both the complete and unit strip models predict the same delamination growth and failure loads with negligible difference. However, the computation effort required by the whole model is significantly greater as the computing time is seven times higher. Comparison of the computational effort of the two models is given in Table 4. Finally, this modelling approach can be applied for through-thickness reinforcement using larger diameter pins or rods in lower areal density.

Conclusions

A new cohesive zone model is developed for evaluating enhanced fracture toughness of z-pinned laminates. Main contributions to the development of predictive models are:

1) Two separate cohesive laws are employed: one for the pins locations and another for the unpinned areas. It has enabled modelling the large scale bridging phenomenon manifested by z-pinned laminates. Once the specific pin bridging law is determined by either testing or modelling, the approach can be used for different pin arrangements.
2) For three pin configurations predicted delamination growth and failure loads using the unit strip model are in excellent agreement with those predicted by the whole model. Computing time for the unit strip model is about 14% of that required by the whole model. Hence, the unit strip model can replace a complete model if pins are placed in a periodical pattern.

3) Prediction is in good agreement with test results in terms of load-displacement relation. However, delamination extension is overestimated by about 20% compared to test measurement.

Acknowledgement

The research is funded by UK Engineering and Physical Sciences Research Council (through the Cranfield University Innovative Manufacturing Research Centre). The authors also thank Prof. IK Partridge and Dr. DDR Cartié for providing experimental test data.

References

1. Dransfield K, Baillie C, Mai Y-W. Improving the delamination resistance of CFRP by stitching - a review. Compos Sci Technol 1994; 50(3): 305-317.
2. Mouritz AP. Review of z-pinned composite laminates. Composites Part A 2007; 38(12): 2383-2397.
3. Cartié DDR, Dell'Anno G, Poulin E, Partridge IK. 3D reinforcement of stiffener-to-skin T-joints by Z-pinning and tufting. Eng Fract Mech 2006; 73(16): 2532-2540.
4. Cartié DDR, Cox BN, Fleck NA. Mechanisms of crack bridging by composite and metallic rods. Composites Part A 2004; 35(11): 1325-1336.
5. Cartié DDR, Troulis M, Partridge IK. Delamination of Z-pinned carbon fibre reinforced laminates. Compos Sci Technol 2006; 66(6): 855-861.
6. Dell'Anno G, Cartié DDR , Partridge IK , Rezai A. Exploring mechanical property balance in tufted carbon fabric/epoxy composites, Composites Part A 2007; 28(11): 2366-2373.
7. Grassi M, Zhang X. Finite element analyses of mode I interlaminar delamination in z-fibre reinforced composite laminates. Compos Sci Technol 2003; 63(12): 1815-1832.
8. Massabo R, Cox BN. Concepts for bridged Mode II delamination cracks. J Mech Phys Solids 1999; 47(6): 1265-1300.
9. Jain LK, Mai Y. On the effect of stitching on mode I delamination toughness of laminated composites. Compos Sci Technol 1994; 51(3): 331-345.
10. Robinson P, Das S. Mode I DCB testing of composite laminates reinforced with z-direction pins: a simple model for the investigation of data reduction strategies. Eng Fract Mech 2004; 71(3): 345-364.
11. Tong L, Sun X. Bending effect of through-thickness reinforcement rods on mode I delamination toughness of DCB specimen – I - Linearly elastic and rigid-perfectly plastic models. Int J Solids Struct2004; 41(24-25): 6831-6852.
12. Byrd LW, Birman V. The estimate of the effect of z-pins on the strain energy release rate, fracture and fatigue in a composite co-cured z-pinned double cantilever beam. Compos Struct 2005; 68(1): 53-63.
13. Ratcliffe JG, O'Brien TK. Discrete spring model for predicting delamination growth in z-fibre reinforced DCB specimens. NASA Report NASA/TM-2004-213019, May 2004.
14. Yan W, Liu H, Mai Y. Numerical study on the mode I delamination toughness of z-pinned laminates. Composites Sci Technol 2003; 63(10): 1481-1493.
15. Yan W, Liu H, Mai Y. Mode II delamination toughness of z-pinned laminates. Composites Sci Technol 2004; 64(13-14): 1937-1945.
16. Grassi M. Numerical modelling of composite laminates with through-thickness-reinforcements. PhD Thesis, Cranfield University, 2004.
17. Dantuluri V, Maiti S, Geubelle PH, Patel R, Kilic H. Cohesive modeling of delamination in Z-pin reinforced composite laminates. Composites Sci Technol 2007; 67(3-4): 616-631.
18. Borg R, Nilsson L, Simonsson K. Simulating DCB, ENF and MMB experiments using shell elements and a cohesive zone model. Composites Sci Technol 2004; 64(2): 269-278.
19. Sun CT, Jin Z-. Modeling of composite fracture using cohesive zone and bridging models. Composites Sci Technol 2006; 66(10): 1297-1302.
20. Diehl T. On using a penalty-based cohesive-zone finite element approach, Part I: Elastic solution benchmarks. Int J Adhes Adhes 2008; 28(4-5): 237-255.

21. Diehl T. On using a penalty-based cohesive-zone finite element approach, Part II: Inelastic peeling of an epoxy-bonded aluminum strip. Int J Adhes Adhes 2008; 28(4-5): 256-265.
22. Guiamatsia I, Ankersen JK, Davies GAO, Iannucci L. Decohesion finite element with enriched basis functions for delamination. Composites Sci Technol 2009; 69(15-16): 2616-2624.
23. Rybicki EF, Kanninen MF. A finite element calculation of stress intensity factors by a modified crack closure integral. Eng Fract Mech 1977; 9(4): 931-938.
24. Wood MDK, Sun X, Tong L, Katzos A, Rispler A, Mai Y. The effect of stitch distribution on Mode I delamination toughness of stitched laminated composites – experimental results and FEA simulation. Compsites Sci Technol 2007; 67(6): 1058-1072.
25. Griffith AA. The Phenomena of rupture and flow in solids. Philosophical Transactions of Royal Society of London 1921; 221: 163-198.
26. Grassi M, Cox B, Zhang X. Simulation of pin-reinforced single-lap composite joints. Composites Sci Technol 2006; 66(11-12): 1623-1638.
27. Meo M, Achard F, Grassi M. Finite element modelling of bridging micro-mechanics in through-thickness reinforced composite laminates. Composite Structures 2005; 71(3-4): 383-387.
28. Cox BN. Snubbing effects in the pullout of a fibrous rod from a laminate. Mech Adv Mater Struct 2005; 12(2): 85-98.
29. Cox BN. A constitutive model for through-thickness reinforcement bridging a delamination crack. Adv Compos Lett 1999; 8(5): 249-256.
30. Cox BN, Sridhar N. A traction law for inclined fiber tows bridging mixed-mode cracks. Mech Adv Mater Struct 2002; 9(4): 299-331.
31. Gray RJ. Analysis of the effect of embedded fibre length on fibre debonding and pull-out from an elastic matrix - Part 1 Review of theories. Journal of materials science 1984; 19(3): 861-870.
32. Liu HY, Yan W, Yu XY, Mai Y-W. Experimental study on effect of loading rate on mode I delamination of z-pin reinforced laminates. Composites Sci Technol 2007; 67(7-8) 1294–1301.

Table 1. Z-pin material properties used for the single-pin pullout model

Z-pin (T300/BMI)

E_{11}	E_{22}	E_{33} (GPa)	G_{12}	G_{13}	G_{23}	ν_{12}	ν_{13}	ν_{23}	α (K^{-1})
100	30	30	4.6	4.6	3.9	0.35	0.35	0.4	0

Table 2. Mechanical properties of IMS/924 [7]

E_1	E_2	E_3 (GPa)	G_{12}	G_{13}	G_{23}	υ_{12}	υ_{13}	υ_{23}	G_{IC} (kJ m^{-2})
138	11	11	4.4	4.4	3.92	0.34	0.34	0.4	0.25

Table 3. Cohesive zone model parameters used in this study

Plain laminate			Pin bridging cohesive law			
K (N/mm^3)	T_0 (MPa)	G_C (kJ/m^2)	Pin diameter: (mm)	K (N/mm^3)	T_0 (MPa)	G_C^{pin} (kJ/m^2)
$1 \cdot 10^5$	30	0.25	0.28	1900	360	240
			0.51	800	160	90

Table 4. Summary of computational efforts of the two models

Case	No. of element		Computational time (hour)	
	unit strip	whole model	unit strip	whole model
Unpinned DCB	–	15k	–	0.5
d = 0.51 mm, A_p = 2%	30k	80k	0.8	6.5
d = 028 mm, A_p = 0.5%	35k	90k	1	7
d = 0.28 mm, A_p = 2%	40k	120k	1.2	–

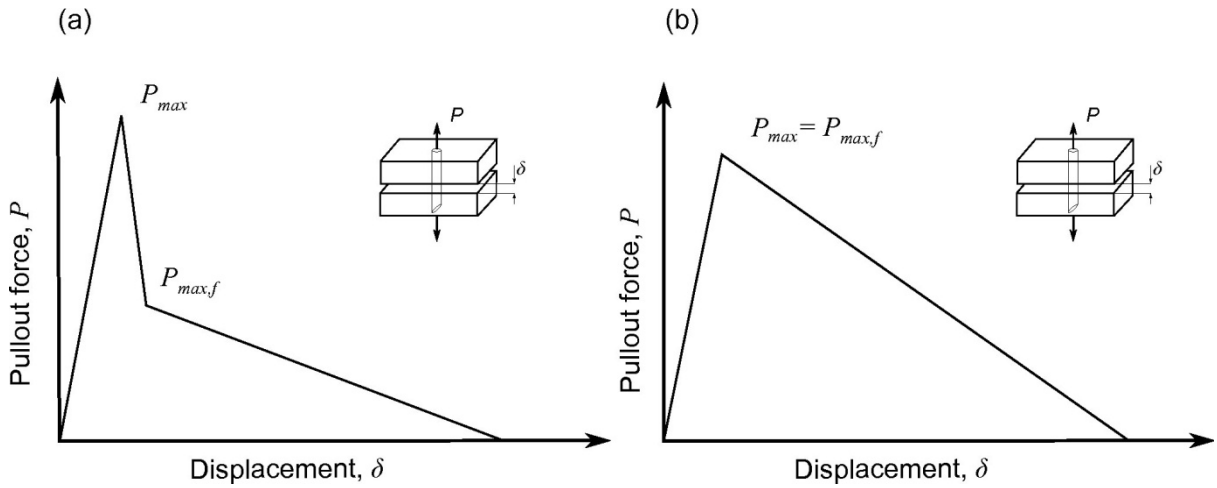

Fig. 1: Pin pullout force vs. crack opening displacement showing two characteristic behaviour of z-pin pullout: (a) low friction resistance, (b) high friction resistance.

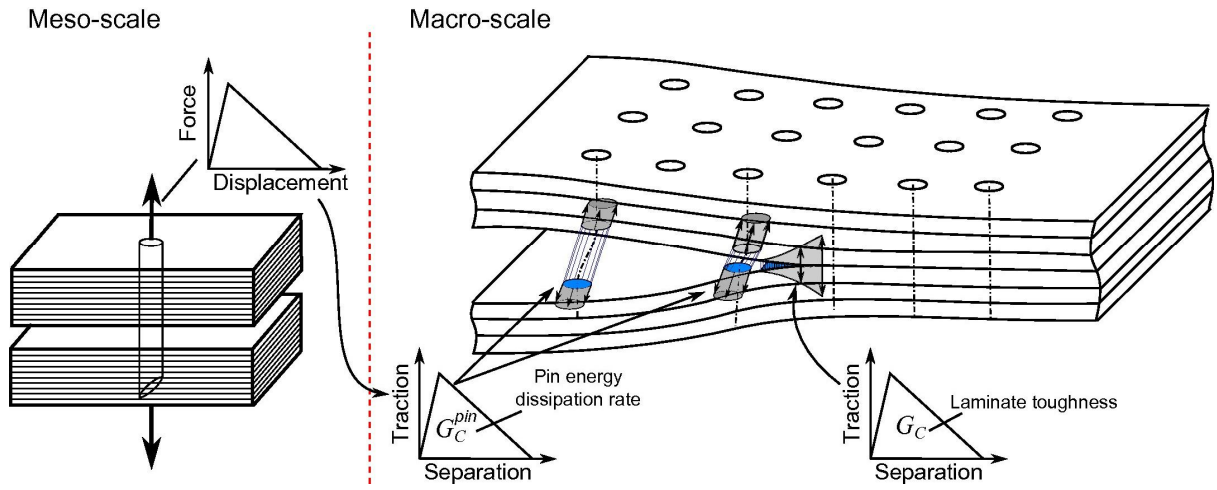

Fig. 2: Modelling strategy using meso and macro-scale models to model delamination of z-pin reinforced laminates.

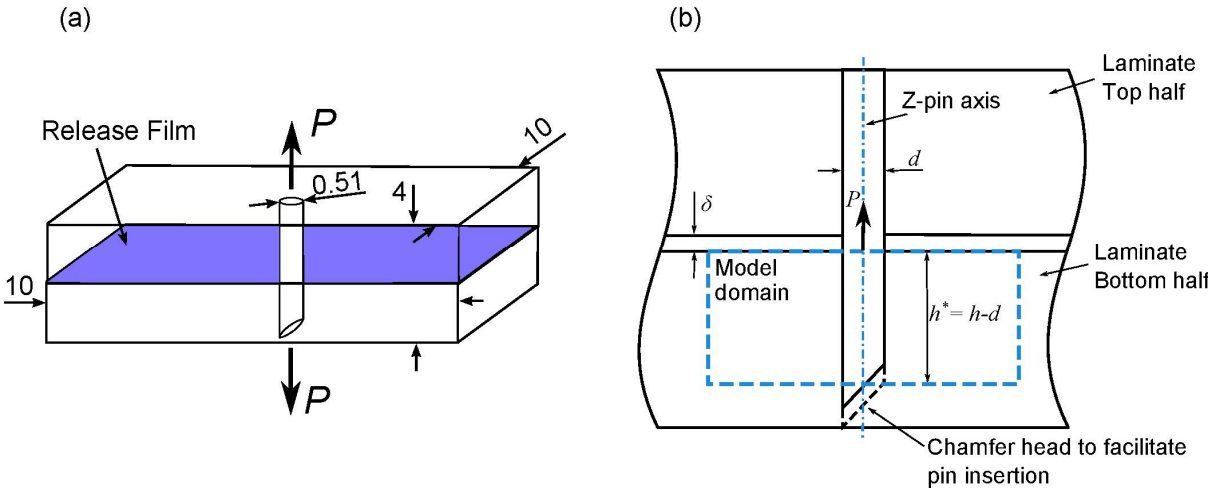

Fig. 3: Geometry of single pin pullout test: (a) schematic of a test specimen; b) FE model domain.

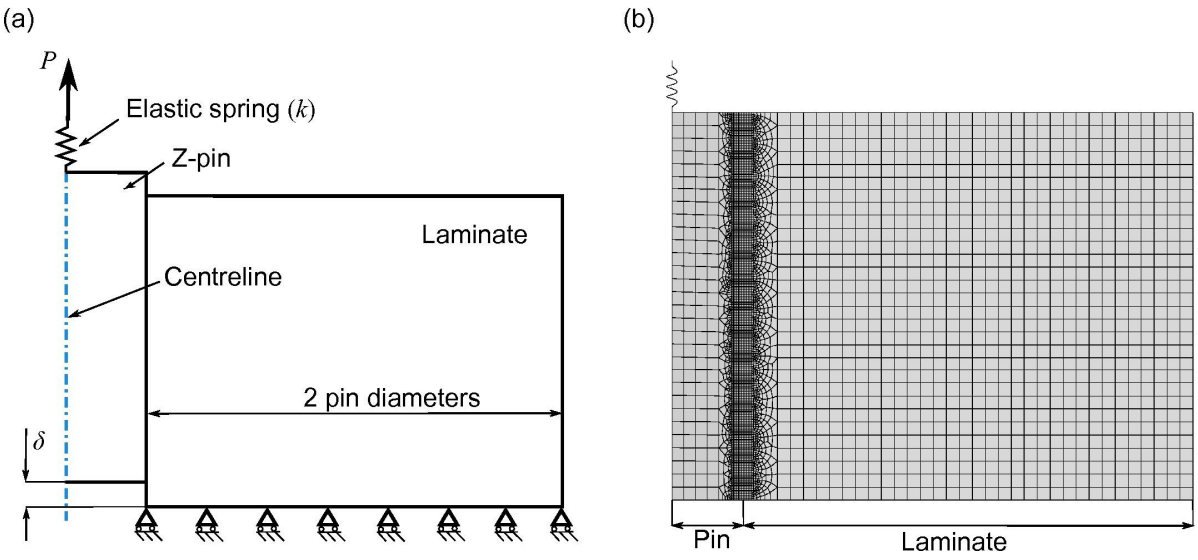

Fig. 4: Meso-scale model: (a) axi-symmetric model and boundary conditions; (b) FE mesh used for the analysis.

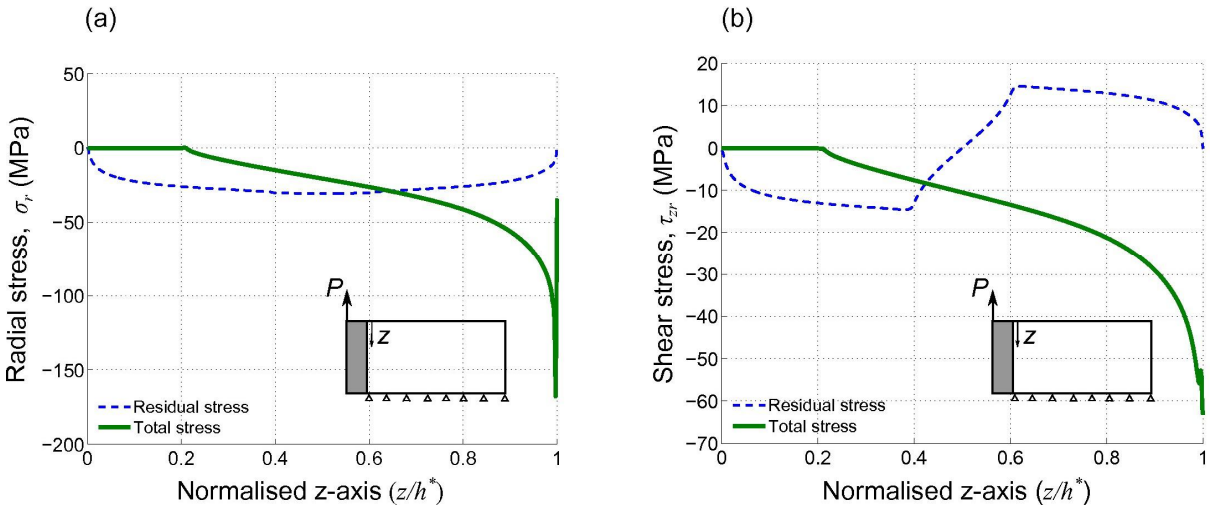

Fig. 5: Stress distribution along the pin at pin/laminate interface: dash line represents thermal residual stress after the curing process, solid line is the total stress at the peak pullout load. (a) Normal (radial) stress, σ_r ; (b) Shear stress, τ_{zr}.

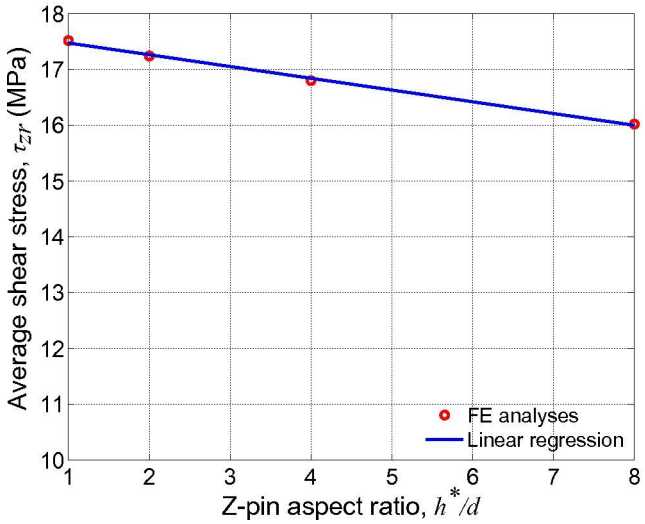

Fig. 6: Influence of z-pin aspect ratio (h^*/d) on the average shear stress.

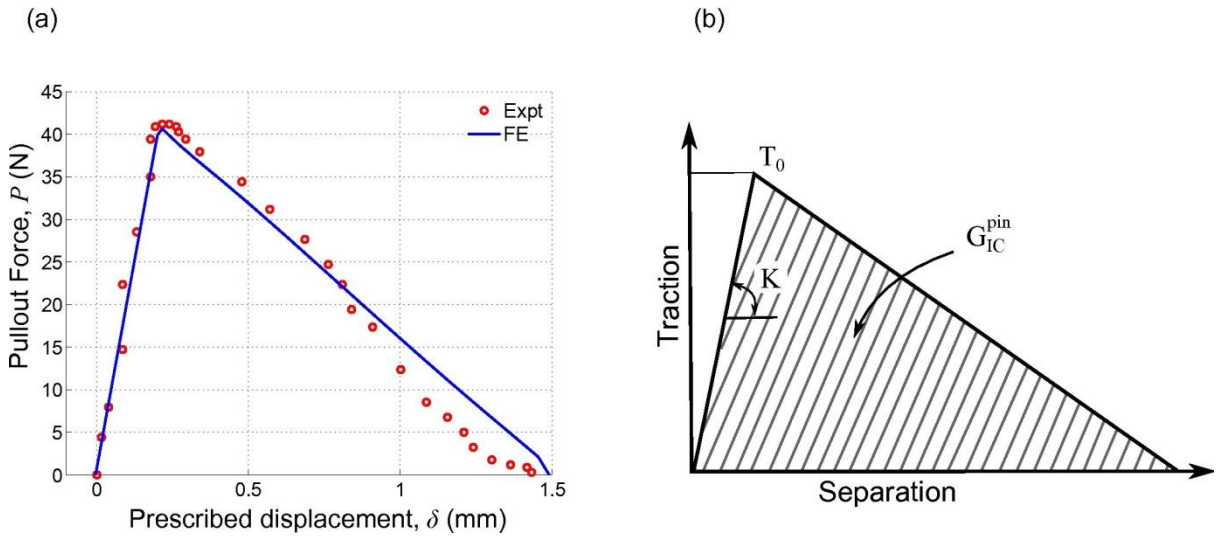

Fig. 7: (a) Pin pullout force vs. displacement – comparison between FE analysis and test measurement [4], (b) schematic of traction-separation law based on the derived force-displacement relation.

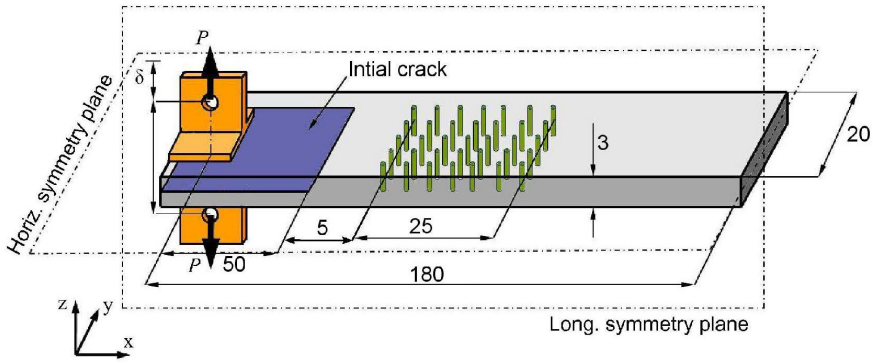

Z-pin parameters

Pinned area (%)	Pin diameter (mm)	Pin Pitch (mm)
2	0.51	3.1
2	0.28	1.55
0.5	0.28	3.5

Fig.8: Geometry and dimension of the z-pinned DCB test specimen (unit: mm).

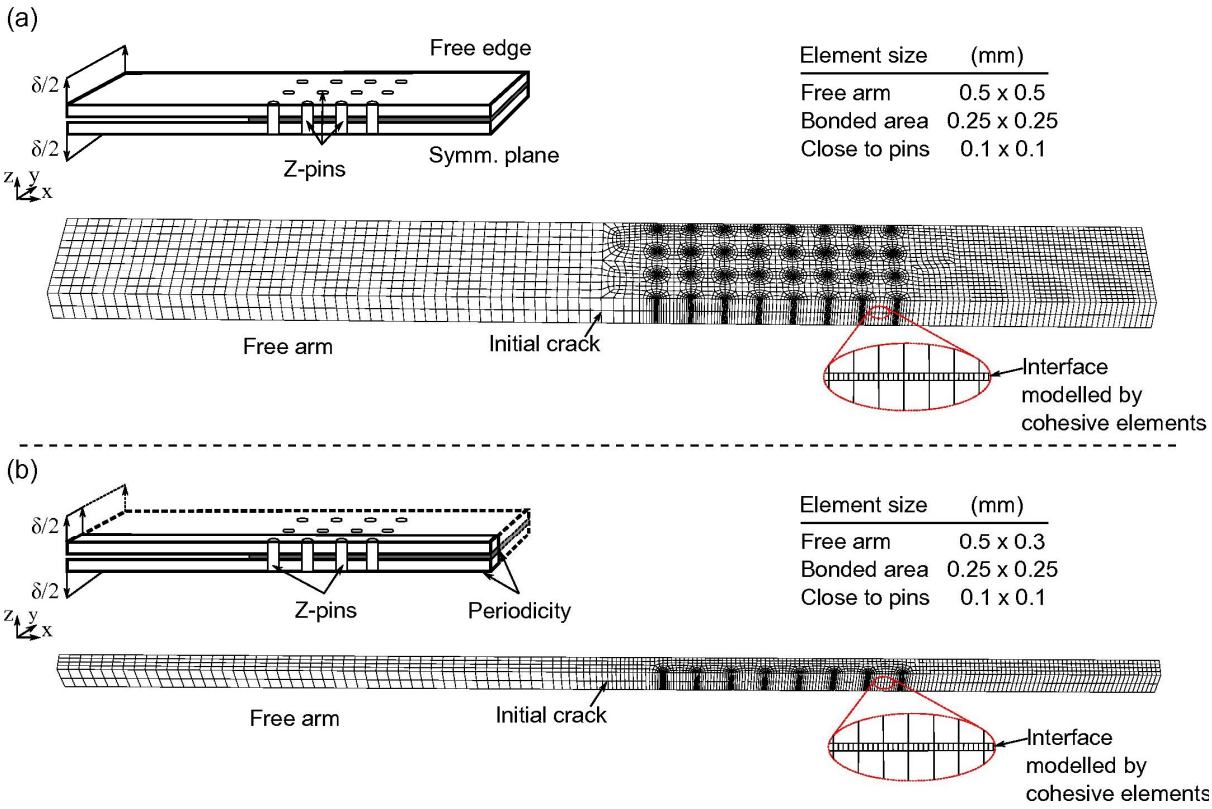

Fig. 9: FE models of DCB specimen using two layers of shell elements and cohesive elements at interface: (a) whole model representing half of the DCB specimen (b) unit strip model for half of a pin row.

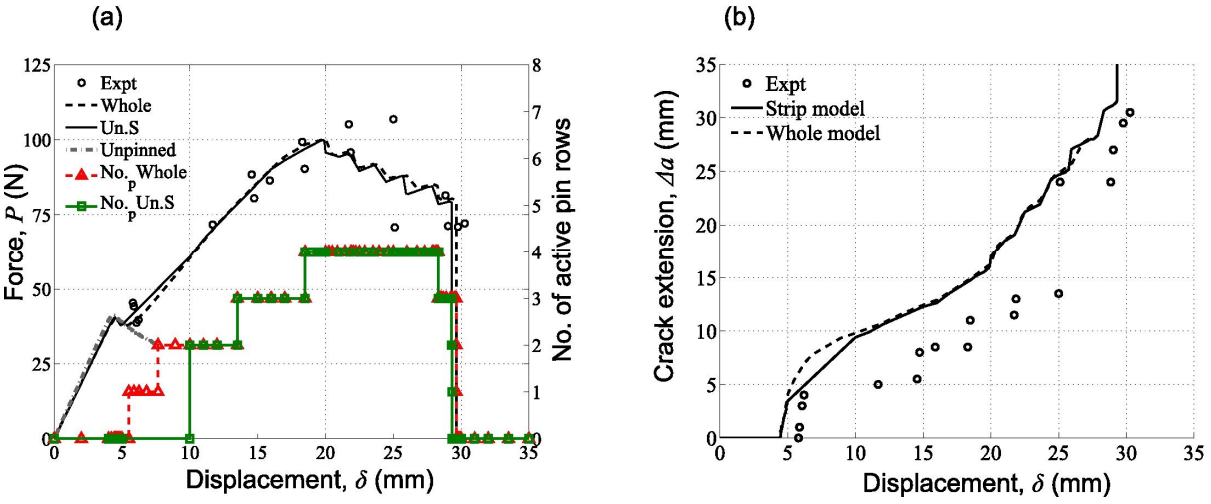

Fig. 10: Comparison between experiment and simulation (pinned laminate: A_p = 2%, d = 0.51 mm), (a) Applied force vs. opening displacement; also showing the number of active pin rows in the crack wake (right-hand y-axis), (b) crack extension vs. opening displacement.

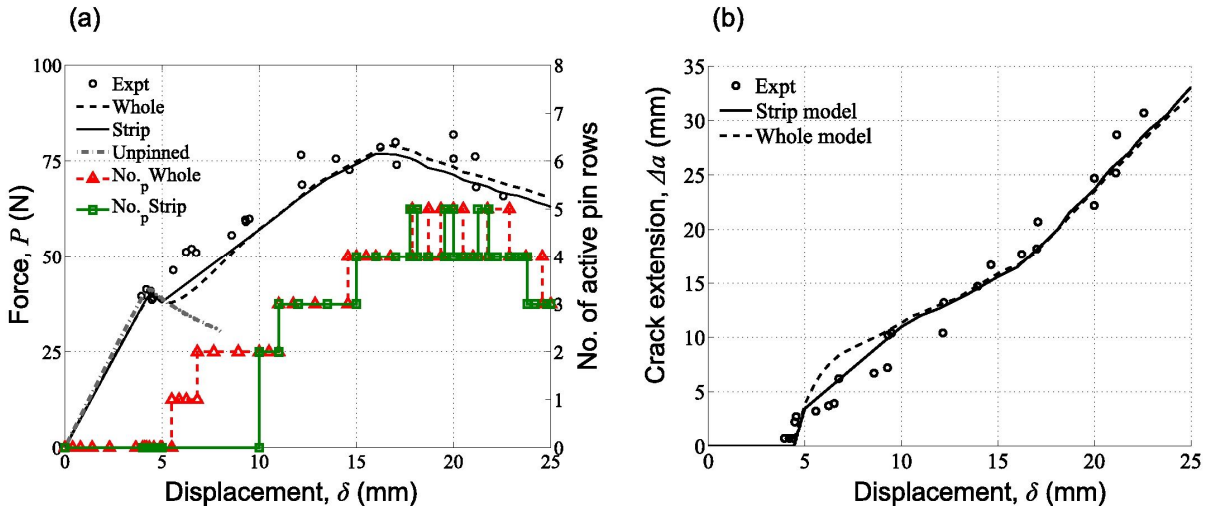

Fig. 11: Comparison between experiment and simulation (pinned laminate: A_p = 0.5%, d = 0.28 mm): (a) Applied force vs. opening displacement; also showing the number of active pin rows in the crack wake (right-hand y-axis), (b) crack extension vs. opening displacement.

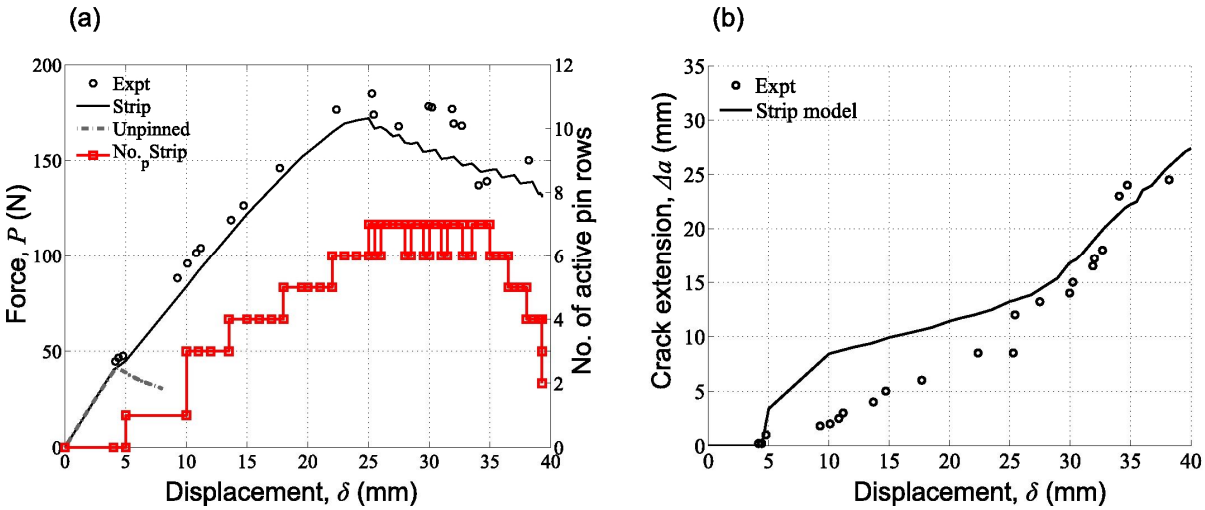

Fig. 12: Comparison between experiment and simulation (pinned laminate: A_p = 2%, d = 0.28 mm): (a) Applied force vs. opening displacement; also showing the number of active pin rows in the crack wake (right-hand y-axis), (b) crack extension vs. opening displacement.

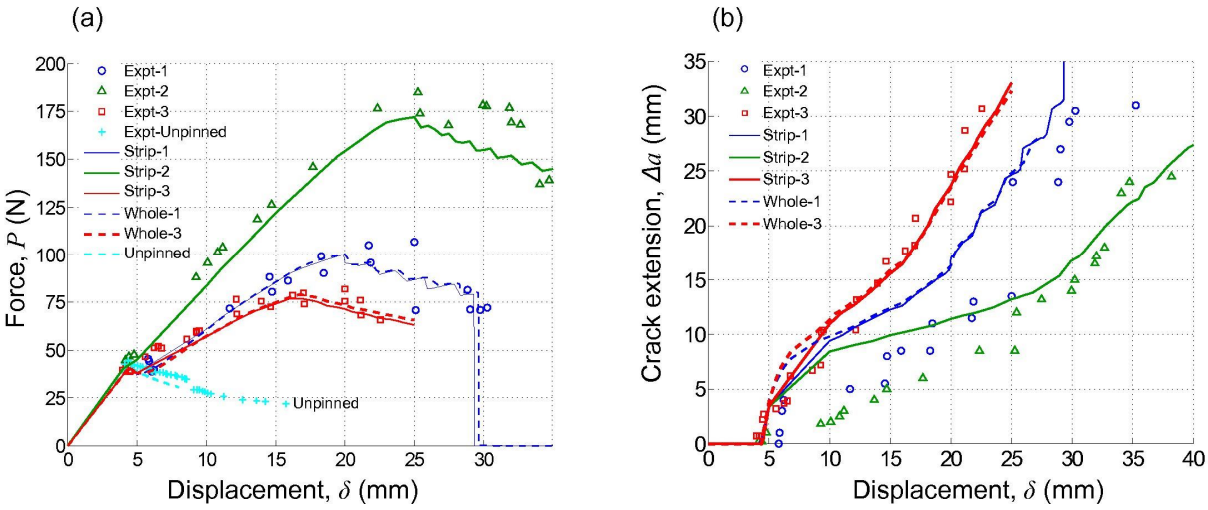

Fig.13: Summary of numerical results: (a) applied force vs. opening displacement, (b) crack extension vs. opening displacement. Plotted configurations: case 1: A_p = 2 %, d = 0.51 mm, case 2: A_p = 2 %, d = 0.28 mm, case 3: A_p = 0.5 %, d = 0.28 mm.

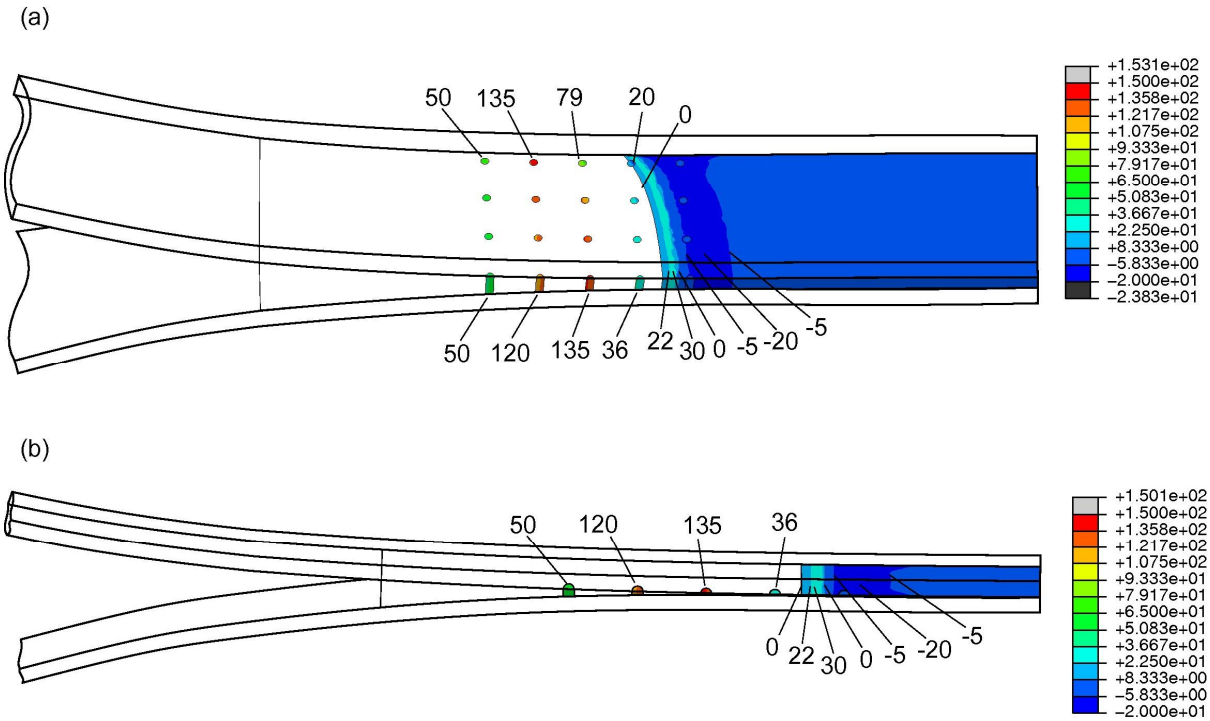

Fig. 14: Peel stresses at interface: (a) whole model, (b) unit strip mode (Unit: MPa).